Eur. Phys. J. C 8, 655–667 (1999)
DOI 10.1007/s100529900007

THE EUROPEAN PHYSICAL JOURNAL C

Off-shell W pair production with anomalous couplings: The CC11 process

J. Biebel, T. Riemann

DESY Zeuthen, Platanenallee 6, D-15738 Zeuthen, Germany

Received: 3 December 1998 / Published online: 22 March 1999

Abstract. The differential cross-sections for processes of the type $e^+e^- \to (W^+W^-) \to l\nu q\bar{q}$ are determined with account of background contributions and of anomalous triple gauge boson couplings. Analytic expressions for $\mathrm{d}\sigma/\mathrm{d}s_1\mathrm{d}s_2\mathrm{d}\cos\theta$, where θ is the production angle of the W boson, are numerically integrated with the Fortran package GENTLE. QED corrections are taken into account in the leading logarithmic approximation. The importance of the various contributions is studied for center-of-mass energies of 190 GeV, 500 GeV, and 1 TeV.

1 Introduction

Since the establishment of the electroweak standard model [1]-[3] many precision tests confirmed its validity in various respects. One of the poorly investigated features is the non-Abelian nature of gauge couplings. W pair production,

$$e^+e^- \to W^+W^-, \tag{1.1}$$

provides an excellent way to investigate the triple gauge boson self couplings.

First calculations of the cross-section for on-shell W pair production in a renormalizable theory, the standard model, were done in the seventies [4,5]. Already before the formulation of the standard model the W width was estimated to yield sizeable effects if the W boson is much heavier than the proton [6]. Due to the finite width, W bosons decay immediately and the production of four fermions is observed. Production of off-shell W pairs,

$$e^+e^- \longrightarrow W^+W^- \longrightarrow \bar{f}_2 f_2' f_1 \bar{f}_1', \tag{1.2}$$

through the three diagrams of Fig. 1 was calculated first in [7]. Feynman diagrams without an intermediate W pair will also contribute to the four fermion final states in (1.2):

$$e^+e^- \longrightarrow f_1\bar{f}_1'\bar{f}_2 f_2'. \tag{1.3}$$

They constitute the so-called irreducible background and are experimentally not distinguishable from the signal diagrams. Classifications and first studies may be found in [8, 9], and an overview in [10]. Further, photonic, electroweak, and QCD radiative corrections must be regarded in order to achieve sufficient accuracy of numerical predictions. A huge literature exists on this subject. See e.g. [11]-[21], and references therein.

The properties of triple boson vertices are investigated with different approaches. Polarization amplitudes for the most general form of the γW^+W^- and ZW^+W^- vertices compatible with Lorentz invariance were determined in [22,23]. Since then, many studies appeared on W pair production with anomalous couplings, see e.g. [24]-[27]. For a recent overview, see e.g. [28].

The study of the physics of W bosons is one of the main goals of LEP 2 and a future high-energy linear collider. LEP 2 operates above the W pair production threshold at about 161 GeV. Several thousands of W pairs will be produced and precise measurements of mass, width, and couplings of the W boson will become possible. Later, at a future linear collider with an energy of 500 GeV or more at high luminosity the number of produced W pairs will be even larger than at LEP 2. For a review see [29].

As mentioned, the process (1.3) may be classified by the final state fermions. In this article, we will treat the CC11 class, defined by two requirements on the final state fermions: (i) they have to belong to two different weak isospin doublets and (ii) no electrons nor electron neutrinos are produced. Besides the doubly resonating diagrams of Fig. 1 there are up to eight background diagrams of the types shown in Fig. 2. This depends on the number of neutrinos in the final state: $l_1\bar{\nu}_1\bar{l}_2\nu_2$, $l_1\bar{\nu}_1\bar{q}q'$, $q_1\bar{q}_1'\bar{q}_2q_2'$, $(l_i \neq e)$. The semi-leptonic CC10 process is of special interest for the study of anomalous couplings since its final states offer the most complete kinematical information for an experimental analysis of W pair production.

Present experimental limits on anomalous couplings are not too stringent. In the parameter space of $\alpha_{W\phi}$, α_W, and $\alpha_{B\phi}$ the combined limits of LEP and D0 are [30] (see also [31,32]) :

$$\begin{aligned} \alpha_{W\phi} &= -0.03^{+0.06}_{-0.06}, \\ \alpha_W &= -0.03^{+0.08}_{-0.08}, \end{aligned} \tag{1.4}$$

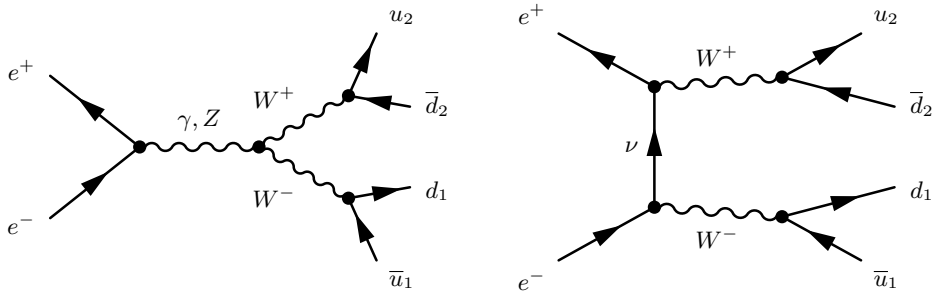

Fig. 1. The doubly resonating CC03 contributions to off-shell W pair production

$$\alpha_{B\phi} = -0.05^{+0.22}_{-0.20}.$$

Here, the identities

$$\alpha_{W\phi} = c_W s_W \delta_Z, \tag{1.5}$$

$$\alpha_W = y_\gamma = \frac{s_W}{c_W} y_Z, \tag{1.6}$$

$$\alpha_{B\phi} = x_\gamma - c_W s_W \delta_Z = -\frac{c_W}{s_W}\left(x_Z + s_W^2 \delta_Z\right) \tag{1.7}$$

are implied, and the anomalous couplings x, y, δ_Z are defined in Sect. 3. These conventions are in accordance with [28,33].

First signals of anomalous triple gauge boson couplings will be small if any. Since the total cross-section is not very sensitive to anomalous couplings, it is advantageous to study distributions.

The semi-analytical expressions of GENTLE for total cross-sections with QED corrections in the standard model were derived for the signal diagrams in [34,35] and for the background contributions in [36,37]. With the results presented in this article, GENTLE may be used also for predictions of $\mathrm{d}\sigma/\mathrm{d}\cos\theta$, where θ is the production angle of one of the W bosons. We present analytical expressions for the *differential cross-section* for processes of the CC11 class in the standard model in Sect. **??** and the effects of *anomalous couplings* in Sect. 3. In appendices we give some technical details of notations and the treatment of QED corrections. Numerical results are discussed in the corresponding sections.

The formulae of this article have been implemented in GENTLE version 2 [38] which is currently used for experimental studies at LEP 2.

2 The angular distribution in the standard model

2.1 The CC03 process

The CC03 process is defined through reaction (1.2). The fermion pairs $f_1\bar{f}_1'$ and $\bar{f}_2 f_2'$ are the decay products of W^- and W^+:

$$W^- \to d_1 \bar{u}'_1, \qquad W^+ \to \bar{d}_2 u'_2, \tag{2.1}$$

and have the invariant masses s_1 and s_2. The scattering angle θ is defined as the angle between the electron and the W^- boson.

The differential cross-section may be written as a sum of s and t-channel contributions and of their interference [7]:

$$\begin{aligned}\frac{\mathrm{d}\sigma_{\mathtt{CC03}}}{\mathrm{d}\cos\theta} = \frac{\sqrt{\lambda}}{2\pi s^2}\int \mathrm{d}s_1\mathrm{d}s_2 \;\big[&\mathcal{C}^t\mathcal{G}^t(s;s_1,s_2,\cos\theta)\\ &+\mathcal{C}^s\mathcal{G}^s(s;s_1,s_2,\cos\theta)\\ &+\mathcal{C}^{st}\mathcal{G}^{st}(s;s_1,s_2,\cos\theta)\big]\,.\end{aligned} \tag{2.2}$$

We give some notations, including the explicit expressions for the $\mathcal{C}$ and $\mathcal{G}$ functions in appendix A.

2.2 Contributions from background diagrams

We subdivide the background contributions into three parts:

$$\frac{\mathrm{d}\sigma_b}{\mathrm{d}\cos\theta} = \frac{\mathrm{d}\sigma_{sb}}{\mathrm{d}\cos\theta} + \frac{\mathrm{d}\sigma_{tb}}{\mathrm{d}\cos\theta} + \frac{\mathrm{d}\sigma_{bb}}{\mathrm{d}\cos\theta}. \tag{2.3}$$

The first term contains the interferences between the two s-channel resonant diagrams and the eight background diagrams. The second one describes the interferences between the t-channel exchange diagram and background, and the third one the pure background contributions.

We denote the various background diagrams by the type of final state fermion coupling to the neutral gauge boson. If e.g. an up-type anti-fermion couples to the photon or the Z boson, we will call this a u_1-diagram. In accordance with (2.1), the subindex 1 (2) indicates by convention that a fermion of the weak doublet with negative (positive) net charge is coupling to the neutral boson. We use the calculational method described in [36] and FORM [39].

2.2.1 Background–s-channel interference

There are 16 interferences between the two s-channel signal diagrams and the eight background diagrams. Each of these interferences is split up into two products $\mathcal{C}_+^{sa_i}\mathcal{G}_+^{sa_i}$ and $\mathcal{C}_-^{sa_i}\mathcal{G}_-^{sa_i}$:

$$\begin{aligned}\frac{\mathrm{d}\sigma_{sb}}{\mathrm{d}\cos\theta} = \frac{\sqrt{\lambda}}{2\pi s^2}\int \mathrm{d}s_1\mathrm{d}s_2 \\ \times \sum_{i=1,2}\sum_{a=u,d}\left[\mathcal{C}_+^{sa_i}\mathcal{G}_+^{sa_i} + \mathcal{C}_-^{sa_i}\mathcal{G}_-^{sa_i}\right].\end{aligned} \tag{2.4}$$

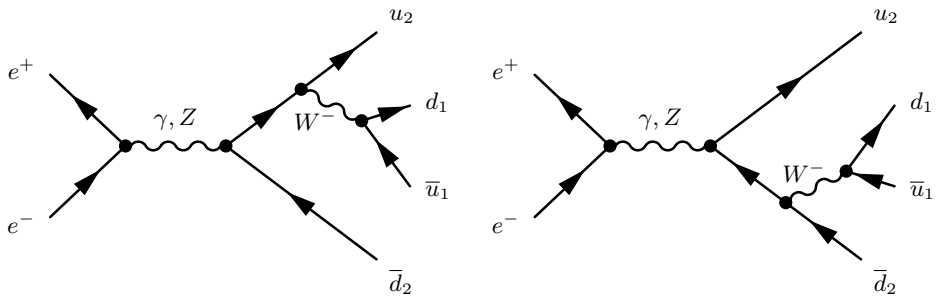

Fig. 2. Four of the eight singly resonant contributions to off-shell W pair production: the d_2-diagrams and the u_2-diagrams

Summation index a stands for up-type or down-type fermions of doublet i. The coefficient functions are:

$$\begin{aligned}\mathcal{C}_{\pm}^{sa_i} = &\sum_{k,l=\gamma,Z}\frac{2}{(6\pi^2)^2}\\ &\times\mathrm{Re}\frac{1}{D_k(s)D_l^*(s)D_W(s_1)D_W(s_2)D_W^*(s_{3-i})}\\ &\times g_k\left[L(e,k)L(e,l)\pm R(e,k)R(e,l)\right]\\ &\times L^2(F_1,W)L^2(F_2,W)L(f_a^i,l)\\ &\times N_c(F_1)N_c(F_2).\end{aligned}\tag{2.5}$$

The propagators are defined in (A.4) and the coupling constants in (A.5). The two independent kinematical functions for the su_1-interference are:

$$\begin{aligned}\mathcal{G}_{-}^{su_1}(s,s_1,s_2) = &\frac{3}{16}\frac{\cos\theta}{\sqrt{\lambda}}ss_2\left\{2s\left[s(s_1+s_2)-s_1^2-s_2^2\right]\right.\\ &\left.\times\,\mathcal{L}(s_1;s_2,s)+(s+s_1)^2-s_2^2\right\},\end{aligned}\tag{2.6}$$

$$\begin{aligned}\mathcal{G}_{+}^{su_1}(s,s_1,s_2) = &\frac{3}{16}\frac{1-3\cos^2\theta}{\lambda}s^2s_1s_2\left[2ss_2\mathcal{L}(s_1;s_2,s)\right.\\ &\left.+s-s_1+s_2\right]\\ &-\frac{3ss_2}{16}\left[s(s_1+s_2)(1+\cos^2\theta)\right.\\ &\left.+2s_1s_2\sin^2\theta\right]\mathcal{L}(s_1;s_2,s)\\ &+\frac{ss_1}{8}(s_1-s-4s_2)\\ &+\frac{3s_2}{32}\left[s(3s_1-s_2-s)(1+\cos^2\theta)\right.\\ &\left.+2s_1(s_1-s_2)\sin^2\theta\right]\\ &+\frac{\lambda\sin^2\theta}{64}(s_1-s-s_2).\end{aligned}\tag{2.7}$$

The logarithm

$$\mathcal{L}(s;s_1,s_2)=\frac{1}{\sqrt{\lambda}}\ln\frac{s-s_1-s_2+\sqrt{\lambda}}{s-s_1-s_2-\sqrt{\lambda}}\tag{2.8}$$

arises from integrating the fermion propagators in the background diagrams.

The $\mathcal{G}_{-}^{sa_i}$-functions are proportional to $\cos\theta$ and, thus, they contribute only to the differential cross-section but do not contribute to the total cross-section. After integration over $\cos\theta$, (2.7) yields (3.1) of [36].

One may obtain the su_2-interference by exchanging s_1 and s_2 in the su_1-interference:

$$\mathcal{G}_{\pm}^{su_2}(s,s_1,s_2)=\mathcal{G}_{\pm}^{su_1}(s,s_2,s_1).\tag{2.9}$$

To construct the kinematical functions with the down-type fermion coupling to the neutral vector boson, one may use the symmetry:

$$\mathcal{G}_{\pm}^{sd_1}(s,s_1,s_2)=\mathcal{G}_{\pm}^{sd_2}(s,s_2,s_1)=\mp\mathcal{G}_{\pm}^{su_1}(s,s_1,s_2).\tag{2.10}$$

The coefficients of the $\mathcal{P}$ violating contributions in (2.4), $\mathcal{C}_{-}^{sa_i}$, vanish for pure photon exchange.

2.2.2 Background–t-channel interference

The t-channel background interference is:

$$\frac{\mathrm{d}\sigma_{tb}}{\mathrm{d}\cos\theta}=\frac{\sqrt{\lambda}}{2\pi s^2}\int\mathrm{d}s_1\mathrm{d}s_2\sum_{i=1,2}\sum_{a=u,d}\mathcal{C}^{ta_i}\mathcal{G}^{ta_i}.\tag{2.11}$$

Due to the neutrino exchange in the t-channel, only left-handed particles contribute and, therefore, only one combination of couplings appears:

$$\begin{aligned}\mathcal{C}^{ta_i} = &\sum_{k=\gamma,Z}\frac{2}{(6\pi^2)^2}\mathrm{Re}\frac{1}{D_W(s_1)D_W(s_2)D_k^*(s)D_W^*(s_{3-i})}\\ &\times L^2(E,W)L(e,k)L(f_i^a,k)L^2(F_1,W)L^2(F_2,W)\\ &\times N_c(F_1)N_c(F_2).\end{aligned}\tag{2.12}$$

The kinematical functions are exceptionally asymmetric since the integration over the fermion propagator in the background diagrams is performed, while the neutrino propagator (A.10) in the t-channel diagram is still present. The kinematical function for the tu_1-interference is:

$$\begin{aligned}&\mathcal{G}^{tu_1}(s,s_1,s_2)=\\ &\frac{-1}{\lambda}\left\{\frac{3}{4}\frac{\cos\theta}{\sqrt{\lambda}}\,s^2s_1s_2^2(5\sin^2\theta-2)\right.\\ &\times\left[\frac{1}{t_\nu}(s+s_1-s_2)+2s\mathcal{L}(s_1;s_2,s)\right]\\ &+\lambda\left[\frac{\sin^2\theta}{8t_\nu}[2s_1s_2(s_2-s_1)\right.\\ &\left.\left.-6s^2s_2(s_1+s_2)\mathcal{L}(s_1;s_2,s)-3ss_2(s+s_2)\right]\right.\end{aligned}$$

$$
\begin{aligned}
&+\frac{\sin^2\theta}{16}[(s-s_1)^2-s_2^2]+\frac{ss_1}{2}\Big]\\
&+\frac{ss_1s_2}{t_\nu}\Big[-\frac{3}{4}ss_2\mathcal{L}(s_1;s_2,s)(5s\sin^4\theta+4s_1+4s_2)\\
&-\frac{1}{8}(3s_2^2-2ss_1+4s_1s_2-7s_1^2+30ss_2+9s^2)\sin^2\theta\\
&-\frac{1}{2}(3s_2^2-2s_1^2-s_1s_2+2ss_1)\Big]+\frac{3s^2s_2}{4}\mathcal{L}(s_1;s_2,s)\\
&\times([4s_1s_2+s_1^2+s_2^2-s(s_1+s_2)]\sin^2\theta\\
&-4[s_1s_2+s_1^2+s_2^2-s(s_1+s_2)])\\
&+\frac{ss_2\sin^2\theta}{8}(2s_1s_2-5s_1^2+3s_2^2-14ss_1-3s^2)\\
&+\frac{s}{2}(5s_1^2s_2-2s_1s_2^2-3s_2^3+5ss_1s_2+3s^2s_2)\Big\}. \qquad (2.13)
\end{aligned}
$$

The expression for the td_1-interference becomes quite compact using (2.13):

$$
\begin{aligned}
\mathcal{G}^{td_1}(s,s_1,s_2)&=-\mathcal{G}^{tu_1}(s,s_1,s_2)\\
&-\frac{3ss_2}{\lambda}\Big[\frac{\sin^2\theta}{4t_\nu}\{(s+s_1+s_2)[s_1(2s_1-s-s_2)\\
&-(s-s_2)^2]-2\left[ss_1(s-s_1)^2+ss_2(s-s_2)^2\right.\\
&\left.+s_1s_2(s_1-s_2)^2\right]\mathcal{L}(s_1;s_2,s)\}\\
&+s\left[s(s_1+s_2)-s_1^2-s_2^2\right]\mathcal{L}(s_1;s_2,s)\\
&+\frac{1}{2}\left[(s+s_1)^2-s_2^2\right]\Big]. \qquad (2.14)
\end{aligned}
$$

The integral over $\cos\theta$ of (2.13) yields $\mathcal{G}^{u,d}_{\texttt{CC11}}$ and of (2.14) yields $\mathcal{G}^{uu,dd}_{\texttt{CC11}}$ ((3.12) in [36]).

The remaining two $\mathcal{G}$ functions are easily constructed:

$$
\mathcal{G}^{tu_2}(s,s_1,s_2)=\mathcal{G}^{tu_1}(s,s_2,s_1) \qquad (2.15)
$$

and

$$
\mathcal{G}^{td_2}(s,s_1,s_2)=\mathcal{G}^{td_1}(s,s_2,s_1). \qquad (2.16)
$$

2.2.3 Pure background

The pure background contribution is:

$$
\begin{aligned}
\frac{\mathrm{d}\sigma_{bb}}{\mathrm{d}\cos\theta}&=\frac{\sqrt{\lambda}}{2\pi s^2}\int \mathrm{d}s_1\mathrm{d}s_2\\
&\times\sum_{a,b=u,d}\sum_{i,j=1,2}\left[\mathcal{C}_+^{a_ib_j}\mathcal{G}_+^{a_ib_j}+\mathcal{C}_-^{a_ib_j}\mathcal{G}_-^{a_ib_j}\right]. \qquad (2.17)
\end{aligned}
$$

Again, we have to introduce additional coefficient functions $\mathcal{C}_-$ compared to the total cross-section, where only $\mathcal{C}_+$ functions appear:

$$
\begin{aligned}
\mathcal{C}_\pm^{a_ib_j}=&\sum_{k,l=\gamma,Z}\frac{2}{(6\pi^2)^2}\mathrm{Re}\frac{1}{D_k(s)D_l^*(s)D_W(s_{3-i})D_W^*(s_{3-j})}\\
&\times[L(e,k)L(e,l)\pm R(e,k)R(e,l)]\\
&\times L^2(F_1,W)L^2(F_2,W)N_c(F_1)N_c(F_2)\\
&\times L(f_i^a,k)L(f_j^b,l). \qquad (2.18)
\end{aligned}
$$

The potentially 2×64 kinematical functions in (2.17) can be reduced to 2×16 functions in a first step since the γ and Z exchange differ only in the coefficient functions (2.18). With

$$
\mathcal{G}_\pm^{a_ib_j}=\mathcal{G}_\pm^{b_ja_i} \qquad (2.19)
$$

the number of independent $\mathcal{G}$-functions is further reduced to 2×10.

Finally, we will need only five kinematical functions to express them all.

The simplest cases are the squares of the various background diagrams ($a=b$ and $i=j$ in (2.17)); they are given by:

$$
\begin{aligned}
\mathcal{G}_-^{u_1u_1}(s,s_1,s_2)=&\frac{3}{4}\frac{\cos\theta}{\sqrt{\lambda}}ss_2\Big\{\frac{1}{2}\mathcal{L}(s_1;s_2,s) \qquad (2.20)\\
&\times\left[(s-s_1)^2-s_2^2\right]+s-s_1-s_2\Big\}
\end{aligned}
$$

and

$$
\begin{aligned}
\mathcal{G}_+^{u_1u_1}(s,s_1,s_2)=&\frac{3}{8}\frac{1-3\cos^2\theta}{\lambda}ss_1s_2^2\left[\mathcal{L}(s_1;s_2,s)\right.\\
&\times(s_2-s_1+s)+2]+\frac{1}{64}\lambda(1-\cos^2\theta)\\
&+\frac{3}{16}s_2(1+\cos^2\theta)\left[s\mathcal{L}(s_1;s_2,s)(s_1-s_2-s)\right.\\
&\left.-2s-s_1\right]+\frac{1}{8}s_1(s+3s_2). \qquad (2.21)
\end{aligned}
$$

By integrating (2.21) over $\cos\theta$ one gets $\mathcal{G}^{ff}_{\texttt{CC11}}$ in (3.3) of [36] while (2.20) vanishes.

The other interferences between background diagrams of the same doublet are:

$$
\mathcal{G}_\pm^{u_2u_2}(s,s_1,s_2)=\mathcal{G}_\pm^{u_1u_1}(s,s_2,s_1), \qquad (2.22)
$$

$$
\mathcal{G}_\pm^{d_1d_1}(s,s_1,s_2)=\pm\mathcal{G}_\pm^{u_1u_1}(s,s_1,s_2), \qquad (2.23)
$$

$$
\mathcal{G}_\pm^{d_2d_2}(s,s_1,s_2)=\pm\mathcal{G}_\pm^{u_1u_1}(s,s_2,s_1). \qquad (2.24)
$$

With the aid of a neutral current function, one may prove the relation:

$$
\begin{aligned}
\mathcal{G}_+^{u_1d_1}(s,s_1,s_2)=&\mathcal{G}_+^{d_1d_1}(s,s_1,s_2)+\mathcal{G}_+^{u_1u_1}(s,s_1,s_2)\\
&-ss_2\mathcal{G}_{422}^{DD}(s,s_1,s_2). \qquad (2.25)
\end{aligned}
$$

The function $\mathcal{G}_{422}^{DD}(s,s_1,s_2)$ may be found in appendix C.

The functions $\mathcal{G}_-^{a_ib_j}$ vanish in the neutral current case and the analogue of (2.25) is:

$$
\begin{aligned}
\mathcal{G}_-^{u_1d_1}(s,s_1,s_2)&=-\left[\mathcal{G}_-^{d_1d_1}(s,s_1,s_2)+\mathcal{G}_-^{u_1u_1}(s,s_1,s_2)\right]\\
&=0. \qquad (2.26)
\end{aligned}
$$

The expressions for the other doublet are:

$$
\mathcal{G}_\pm^{u_2d_2}(s,s_1,s_2)=\mathcal{G}_\pm^{u_1d_1}(s,s_2,s_1). \qquad (2.27)
$$

The interferences between diagrams from different doublets are more complicated. Here, we have

$$\mathcal{G}_{-}^{u_1 d_2}(s,s_1,s_2) = \frac{3}{8}\frac{\cos\theta}{\sqrt{\lambda}} s \left\{ 2s \left[s_2^2 \mathcal{L}(s_1;s_2,s) - s_1^2 \mathcal{L}(s_2;s,s_1) + \frac{s_2-s_1}{2} \right] - s_1^2 + s_2^2 \right\} \tag{2.28}$$

and the lengthy expressions

$$\begin{aligned}
\mathcal{G}_{+}^{u_1 d_2}(s,s_1,s_2) &= -18\frac{s^2 s_1^2 s_2^2}{\lambda^3}(1+\sin^2\theta) s^2 s_1 s_2 \mathcal{L}(s_1;s_2,s) \\
&\times \mathcal{L}(s_2;s,s_1) - 3s\left[s_1^2 \mathcal{L}(s_2;s,s_1) + s_2^2 \mathcal{L}(s_1;s_2,s) \right] \\
&\times \left[\frac{\sin^2\theta}{8} + \frac{s\cos^2\theta}{4\lambda}(s-\sigma) + \frac{s^2 s_1 s_2 (1+\sin^2\theta)}{2\lambda^2} \right. \\
&\times \left. \left(2 - 3s\frac{s-3\sigma}{\lambda} \right) \right] - s(s_1-s_2) \\
&\times \left[s_1^2 \mathcal{L}(s_2;s,s_1) - s_2^2 \mathcal{L}(s_1;s_2,s) \right] \\
&\times \left[\frac{3\sin^2\theta}{8\lambda}(s-\sigma) + \frac{3s s_1 s_2 (1+\sin^2\theta)}{2\lambda^2} \right. \\
&\times \left. \left(1 - 3s\frac{s+\sigma}{\lambda} \right) \right] + \frac{3s^2 s_1 s_2 (1+\sin^2\theta)}{4\lambda^2} \\
&\times \left[s^2 - s_1^2 - s_2^2 - \frac{12 s s_1 s_2 (s-\sigma)}{\lambda} \right] \\
&+ \frac{s(1+\cos^2\theta)}{16\lambda} \left[4 s s_1 s_2 + 3(s_1^3 + s_2^3) \right. \\
&\left. - (3s^2 + 7 s_1 s_2)\sigma \right] - \frac{\sin^2\theta}{32} \left[\frac{24 s s_1 s_2 (2s-\sigma)}{\lambda} \right. \\
&\left. + s^2 - s_1^2 - s_2^2 - 10 s_1 s_2 \right]
\end{aligned} \tag{2.29}$$

and

$$\begin{aligned}
\mathcal{G}_{-}^{u_1 u_2}(s,s_1,s_2) &= -\mathcal{G}_{-}^{u_1 d_2}(s,s_1,s_2) + \frac{s\cos\theta}{\sqrt{\lambda}} \left\{ \frac{27 s^2 s_1^2 s_2^2}{2\lambda^2} \right. \\
&\times \left[s(\sigma-s)\mathcal{L}(s_1;s_2,s)\mathcal{L}(s_2;s,s_1) + (s_1 - s - s_2) \right. \\
&\left. \times \mathcal{L}(s_1;s_2,s) + (s_2 - s - s_1)\mathcal{L}(s_2;s,s_1) - 2 \right] \\
&+ \frac{9 s s_1 s_2}{2\lambda} \left[s[3 s_1 s_2 + s(\sigma-s)]\mathcal{L}(s_1;s_2,s)\mathcal{L}(s_2;s,s_1) \right. \\
&+ \left[s(s_1-s) + s_2\left(s_1 - s_2 - \frac{s}{2} \right) \right] \mathcal{L}(s_1;s_2,s) \\
&\left. + \left[s_2(s_2 - s - s_1) - \frac{5}{2} s s_1 \right] \mathcal{L}(s_2;s,s_1) - \frac{5}{4}(s+\sigma) \right] \\
&+ \frac{3 s_1}{4} \left[6 s^2 s_2 \mathcal{L}(s_1;s_2,s)\mathcal{L}(s_2;s,s_1) + 3 s s_2 \mathcal{L}(s_1;s_2,s) \right. \\
&\left. \left. - s(3s_2 + 2s_1)\mathcal{L}(s_2;s,s_1) - \left(s + s_1 + \frac{3}{2} s_2 \right) \right] \right\}.
\end{aligned} \tag{2.30}$$

In (2.29) and (2.30) we use the abbreviation

$$\sigma = s_1 + s_2. \tag{2.31}$$

Further,

$$\mathcal{G}_{+}^{u_1 u_2}(s,s_1,s_2) = \frac{1}{2} s s_1 s_2 \mathcal{G}_{233}^{DD}(\cos\theta,s,s_1,s_2) - \mathcal{G}_{+}^{u_1 d_2}(s,s_1,s_2). \tag{2.32}$$

The neutral current function $\mathcal{G}_{233}^{DD}(\cos\theta,s,s_1,s_2)$ can be found in appendix C. The integral of (2.29) is $\mathcal{G}_{\texttt{CC11}}^{u,d}$ defined in (3.10) of [36] and that of (2.28) and (2.30) vanish.

The remaining kinematical functions are

$$\mathcal{G}_{\pm}^{d_1 u_2}(s,s_1,s_2) = \mathcal{G}_{\pm}^{u_1 d_2}(s,s_2,s_1) \tag{2.33}$$

and

$$\mathcal{G}_{\pm}^{d_1 d_2}(s,s_1,s_2) = \pm\mathcal{G}_{\pm}^{u_1 u_2}(s,s_1,s_2). \tag{2.34}$$

2.3 Numerical results

Numerical results are obtained with the Fortran program GENTLE [38], version 2.02.
QED initial state radiation (ISR) is treated as described in appendix B and in [38].

We use the numerical default input values, e.g. $M_W = 80.230$ GeV, $\Gamma_W = 2.0855$ GeV, $M_Z = 91.1888$ GeV, $\Gamma_Z = 2.4974$ GeV, $\sin^2\theta_W = 0.22591$, $\alpha_{em} = 1/137.0359895$, $\alpha_s = 0.12$, no Cabibbo mixing, and the GENTLE flag settings

IPROC = IINPT = IONSHL = IZETTA = 1
ICONVL = IIQCD = IDCS = IMAP = IRSTP =
IMMIN = IMMAX = 1
IGAMWS = IGAMZS = 1
IGAMW = ITNONU = IQEDHS = ICOLMB = IZERO =
IBIN = IRMAX = 0.

The flags IBORNF, IBCKGR, ICHNNL are varied in an obvious way. For calculations within the standard model IANO is set equal to 0. The flags IGAMWS and IGAMZS are chosen such that the boson widths are taken to be constant. For the related problems with gauge invariance see [40,41,10].

In Fig. 3 the net size of the background effects at a center-of-mass energy of 500 GeV is shown as the ratio of the signal plus background cross-section to the signal cross-section

$$R = \frac{\mathrm{d}\sigma_{\texttt{CC11}}/\mathrm{d}\cos\theta}{\mathrm{d}\sigma_{\texttt{CC03}}/\mathrm{d}\cos\theta}. \tag{2.35}$$

The background contributions may become sizeable for large scattering angles. For extreme backward production, $\cos\theta = -1$, the effect is larger than 30%. At $\sqrt{s} = 190$ GeV, $\mathrm{d}\sigma_b/\mathrm{d}\cos\theta$ (see (2.3) is less than 0.3% of $\sigma_{\texttt{CC03}}$ in the whole range of the scattering angle; for more details see [42].

In Tables 1 and 2 we present numerical data which may be of some use for precision comparisons of different numerical programs. For this purpose, we ran GENTLE at high numerical precision but still a reasonable computing time at a PC with a Pentium 133 MHz processor. The numerical reliability was controlled by varying the parameters

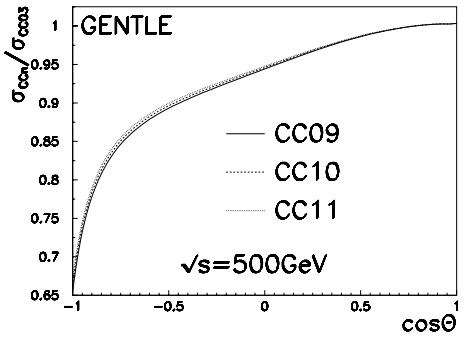

Fig. 3. The ratios CC09/CC03, CC10/CC03, and CC11/CC03 without QED corrections

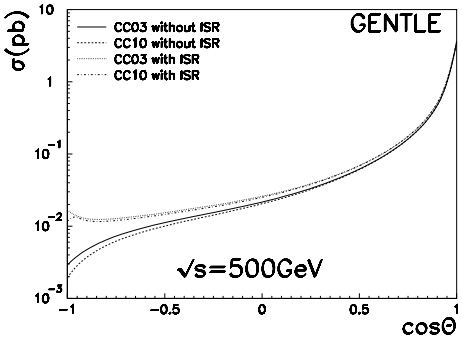

Fig. 4. Differential cross-section for $e^+e^- \to \mu^-\bar{\nu}_\mu u\bar{d}$ with various corrections

ϵ (for the relative error of Simpson integration) and δ (a technical cut parameter improving numerical stability in some edges of the phase space) in GENTLE. The *technical uncertainties* in the last digits shown in the tables are of the order one or smaller. Without ISR the cross-sections are obtained with $\epsilon = 10^{-8}$ and $\delta = 10^{-5}$. With ISR, the corresponding values are $\epsilon = 3 \times 10^{-5}$ and $\delta = 10^{-4}$ (if IBCKGR=1 and IBORNF=1, then $\delta = 10^{-3}$).

Although there are different coupling constants and even a different number of contributing diagrams for the various CC09, CC10, CC11 processes, one observes only small differences between the various cross-sections, especially at LEP 2 energies. One may suspect that this is due to certain relations between the relevant coupling constant combinations in the cross-sections which make the latter being dependent on only weak iso-spins. For example, the s-channel background interference contributions $\mathcal{C}_+^{su_i}\mathcal{G}_+^{su_i} + \mathcal{C}_+^{sd_i}\mathcal{G}_+^{sd_i}$ are identical for all processes of the CC11 class. Here, only the parity violating terms lead to different background effects in this interference. Similarly, for the t-channel background interference the flavour depending combination $\mathcal{G}^{tu_i} + \mathcal{G}^{td_i}$ is suppressed by cancellations as it can be seen in (2.14). Obviously, the effects which are similar for all final states of the CC11 class are the numerically dominating background corrections.

QED corrections are shown in Fig. 4 at $\sqrt{s} = 500$ GeV. There is a considerable cross-section enhancement for $\cos\theta < -0.5$. The background effect in this region of $\cos\theta$ is reduced, but still sizeable.

3 Anomalous couplings

We now extend the Lagrangian of the standard model by anomalous triple gauge boson couplings. We allow terms that obey Lorentz invariance and $\mathcal{CP}$ invariance. In addition, for the electromagnetic interaction we forbid $\mathcal{C}$ or $\mathcal{P}$ violation and will not modify its strength.

These conditions are fulfilled by the Lagrangian proposed in [43]:

$$\begin{aligned}\mathcal{L} = &-ie\left[A_\mu\left(W^{-\mu\nu}W^+_\nu - W^{+\mu\nu}W^-_\nu\right) + F_{\mu\nu}W^{+\mu}W^{-\nu}\right]\\ &- iex_\gamma F_{\mu\nu}W^{+\mu}W^{-\nu}\\ &-ie\cot\Theta_w\left[Z_\mu\left(W^{-\mu\nu}W^+_\nu - W^{+\mu\nu}W^-_\nu\right)\right.\\ &\left.+Z_{\mu\nu}W^{+\mu}W^{-\nu}\right] - iex_Z Z_{\mu\nu}W^{+\mu}W^{-\nu}\\ &- ie\delta_Z\left[Z_\mu\left(W^{-\mu\nu}W^+_\nu - W^{+\mu\nu}W^-_\nu\right)\right.\\ &\left.+Z_{\mu\nu}W^{+\mu}W^{-\nu}\right]\\ &- ie\frac{y_\gamma}{M_W^2}F^{\nu\lambda}W^-_{\lambda\mu}W^{+\mu}_\nu - ie\frac{y_Z}{M_W^2}Z^{\nu\lambda}W^-_{\lambda\mu}W^{+\mu}_\nu\\ &+\frac{ez_Z}{M_W^2}\partial_\alpha\tilde{Z}_{\rho\sigma}\left(\partial^\rho W^{-\sigma}W^{+\alpha}\right.\\ &\left.-\partial^\rho W^{-\alpha}W^{+\sigma} + \partial^\rho W^{+\sigma}W^{-\alpha} - \partial^\rho W^{+\alpha}W^{-\sigma}\right).\end{aligned} \tag{3.1}$$

The term with the dual field tensor $\tilde{Z}$ violates both $\mathcal{C}$ and $\mathcal{P}$. With a multipole expansion, one gets the electromagnetic charge Q_W, the magnetic dipole moment μ_W, and the electric quadrupole moment q_W [44,28]:

$$Q_W = e, \tag{3.2}$$

$$\mu_W = \frac{e}{2M_W}(2 + x_\gamma + y_\gamma), \tag{3.3}$$

$$q_W = -\frac{e}{M_W^2}(1 + x_\gamma - y_\gamma). \tag{3.4}$$

The anomalous couplings x_γ, x_Z, y_γ, y_Z, z_Z, and δ_Z produce additional contributions to the cross-section of W pair production. The largest contributions will come from resonant diagrams (Sect. 3.1), but others are also coming from the interference between anomalous s-channel signal diagrams and background (Sect. 3.2).

3.1 Anomalous contributions to the CC03 process

We write the cross-section for doubly resonant scattering with anomalous couplings in the following form:

$$\frac{\mathrm{d}\sigma^{\mathrm{ano}}_{\mathrm{CC03}}}{\mathrm{d}\cos\theta} = \frac{\sqrt{\lambda}}{2\pi s^2}\int \mathrm{d}s_1\mathrm{d}s_2\left[\sum_{nm}\mathcal{C}^s_{nm}\mathcal{G}^s_{nm}(s;s_1,s_2,\cos\theta)\right.$$
$$\left.+\sum_n \mathcal{C}^{st}_n\mathcal{G}^{st}_n(s;s_1,s_2,\cos\theta)\right]. \tag{3.5}$$

The sums over n,m run over x, y, δ, and z and the standard model couplings. The first sum in (3.5) describes the s-channel interferences and the second sum the anomalous

Table 1. Differential cross-sections without ISR. The CC03 cross-section is calculated with the branching ratios for the CC10 process

$\sqrt{s}$ (GeV)	$\cos\theta$	$\sigma_{\texttt{CC03}}$ (pb)	$\sigma_{\texttt{CC09}}$ (pb)	$\sigma_{\texttt{CC10}}$ (pb)	$\sigma_{\texttt{CC11}}$ (pb)
190	–0.8	0.0943803	0.0303466	0.0945159	0.294360
	0.0	0.216791	0.0697497	0.217241	0.676600
	0.8	0.790432	0.253951	0.791012	2.46385
500	–0.8	0.00646155	0.00172150	0.00539258	0.0168880
	0.0	0.0215908	0.00654501	0.0204228	0.0637232
	0.8	0.212368	0.0682179	0.212503	0.661957
1000	–0.8	0.00244188	0.000403725	0.00128268	0.00407275
	0.0	0.00614750	0.00155423	0.00484706	0.0151154
	0.8	0.0535172	0.0170530	0.0530947	0.165310

Table 2. Differential cross-sections with ISR. The CC03 cross-section is calculated with the branching ratios for the CC10 process

$\sqrt{s}$ (GeV)	$\cos\theta$	$\sigma_{\texttt{CC03}}$ (pb)	$\sigma_{\texttt{CC09}}$ (pb)	$\sigma_{\texttt{CC10}}$ (pb)	$\sigma_{\texttt{CC11}}$ (pb)
190	–0.8	0.09064	0.02915	0.09077	0.2827
	0.0	0.1971	0.06340	0.1975	0.6150
	0.8	0.6868	0.2206	0.6871	2.140
500	–0.8	0.01248	0.003749	0.01170	0.0365
	0.0	0.02590	0.008036	0.02506	0.0782
	0.8	0.2308	0.07418	0.2311	0.7198
1000	–0.8	0.005282	0.001441	0.004510	0.01412
	0.0	0.007757	0.00223	0.006939	0.02163
	0.8	0.0613	0.01963	0.06114	0.1904

st-interferences. The coefficient functions are:

$$\mathcal{C}^s_{nm} = \sum_{k,l=\gamma,Z} \frac{2}{(6\pi^2)^2}\mathrm{Re}\frac{1}{|D_W(s_1)|^2|D_W(s_2)|^2 D_k(s)D^*_l(s)} \times g^n_k g^m_l[1+(1-\delta^n_m)\delta^k_l]A^{nm}_{kl} \times L^2(F_1,W)L^2(F_2,W)N_c(F_1)N_c(F_2), \quad (3.6)$$

$$\mathcal{C}^{st}_n = \sum_{k=\gamma,Z} \frac{2}{(6\pi^2)^2}\mathrm{Re}\frac{1}{|D_W(s_1)|^2|D_W(s_2)|^2 D_k(s)} \times g^n_k L(e,l)L^2(F_1,W)L^2(F_2,W)L^2(e,W) \times N_c(F_1)N_c(F_2), \quad (3.7)$$

with

$$g^x_\gamma = g s_W x_\gamma, \qquad g^x_Z = g s_W x_Z,$$
$$g^y_\gamma = \frac{g s_W y_\gamma}{M^2_W}, \qquad g^y_Z = \frac{g s_W y_Z}{M^2_W}, \quad (3.8)$$
$$g^\delta_Z = g s_W \delta_Z, \qquad g^z_Z = \frac{g s_W z_Z}{M^2_W}.$$

and the standard model couplings

$$g^{\mathrm{SM}}_\gamma = g s_W, \qquad g^{\mathrm{SM}}_Z = g c_W. \quad (3.9)$$

The constant A^{nm}_{kl} is defined as follows:

$$A^{zm}_{kl} = A^{mz}_{kl} = L(e,k)L(e,l) - R(e,k)R(e,l) \quad \text{for } m \neq z \quad (3.10)$$

$$A^{nm}_{kl} = L(e,k)L(e,l) + R(e,k)R(e,l) \quad \text{otherwise} \quad (3.11)$$

The δ^l_k in (3.6) is the Kronecker symbol. Note that the pure standard model contributions are already treated in Sect. 2.1 and should not be counted twice.

The anomalous kinematic functions in (3.5) are for the st-interference:

$$\mathcal{G}^{st}_x = \frac{1}{8}s\left[(s_1+s_2)\left(s-s_1-s_2-\frac{2s_1s_2}{t_\nu}\right) + \frac{\lambda}{4}\sin^2\theta\right], \quad (3.12)$$

$$\mathcal{G}^{st}_y = \frac{1}{4}s s_1 s_2\left[s-s_1-s_2-\frac{2s_1s_2}{t_\nu}\right], \quad (3.13)$$

$$\mathcal{G}^{st}_z = \frac{1}{16}\lambda s\left[2(s_1+s_2)-\frac{\sin^2\theta}{t_\nu}(s_1(s-s_1) + s_2(s-s_2))\right], \quad (3.14)$$

while for the s-channel contributions:

$$\mathcal{G}^s_{xx} = \frac{1}{128}\lambda s\left[(s_1+s_2)(1+\cos^2\theta)\right.$$

$$+s\sin^2\theta\big]\,, \tag{3.15}$$

$$\mathcal{G}^s_{xy} = \frac{1}{64}\lambda s s_1 s_2(1+\cos^2\theta), \tag{3.16}$$

$$\mathcal{G}^s_{sx} = \mathcal{G}^s_{x\delta} = \frac{1}{128}\lambda s\,[4(s_1+s_2) +(s-s_1-s_2)\sin^2\theta\big]\,, \tag{3.17}$$

$$\mathcal{G}^s_{yy} = \frac{1}{128}\lambda s s_1 s_2\,\big[2s\sin^2\theta +(s_1+s_2)(1+\cos^2\theta)\big]\,, \tag{3.18}$$

$$\mathcal{G}^s_{sy} = \mathcal{G}^s_{y\delta} = \frac{1}{16}\lambda s s_1 s_2, \tag{3.19}$$

$$\mathcal{G}^s_{zz} = \frac{1}{128}\lambda^2 s(s_1+s_2)(1+\cos^2\theta), \tag{3.20}$$

$$\mathcal{G}^s_{s\delta} = \mathcal{G}^s_{\delta\delta} = \frac{1}{32}\lambda\left[2s(s_1+s_2) +\left(3s_1s_2+\frac{\lambda}{4}\right)\sin^2\theta\right], \tag{3.21}$$

$$\mathcal{G}^s_{xz} = \frac{1}{64}\lambda^{\frac{3}{2}} s(s_1+s_2)\cos\theta, \tag{3.22}$$

$$\mathcal{G}^s_{yz} = \frac{1}{32}\lambda^{\frac{3}{2}} s s_1 s_2\cos\theta, \tag{3.23}$$

$$\mathcal{G}^s_{sz} = \mathcal{G}^s_{z\delta} = -\frac{1}{32}\lambda^{\frac{3}{2}} s(s_1+s_2)\cos\theta. \tag{3.24}$$

3.2 Interferences of anomalous contributions with background

Finally, we treat interferences of the anomalous s-channel diagrams with background:

$$\frac{\mathrm{d}\sigma^{\mathrm{ano}}_{sb}}{\mathrm{d}\cos\theta} = \frac{\sqrt{\lambda}}{2\pi s^2}\int \mathrm{d}s_1\mathrm{d}s_2 \times \sum_{a=u,d}\sum_{i=1,2}\sum_n \left[\mathcal{C}^{sa_i}_{+,n}\mathcal{G}^{sa_i}_{+,n} + \mathcal{C}^{sa_i}_{-,n}\mathcal{G}^{sa_i}_{-,n}\right]. \tag{3.25}$$

The coefficient functions are

$$\begin{aligned}\mathcal{C}^{sa_i}_{\pm,n} = &\sum_{k,l=\gamma,Z}\frac{2}{(6\pi^2)^2}\\ &\times\mathrm{Re}\frac{1}{D_k(s)D_l^*(s)D_W(s_1)D_W(s_2)D_W^*(s_{3-i})}\\ &\times g^n_k\left[L(e,k)L(e,l)\pm R(e,k)R(e,l)\right]\\ &\times L^2(F_1,W)L^2(F_2,W)L(f^i_a,l)\\ &\times N_c(F_1)N_c(F_2),\end{aligned} \tag{3.26}$$

where g^n_k stands for all couplings given in (3.8).

The anomalous kinematical functions are:

$$\mathcal{G}^{su_1}_{-,x}(s,s_1,s_2) = \frac{3}{32}\frac{\cos\theta}{\sqrt{\lambda}}ss_2\left\{2s[s(s_1+s_2)-s_1^2-s_2^2] \times\mathcal{L}(s_1;s_2,s)+(s+s_1)^2-s_2^2\right\}, \tag{3.27}$$

$$\begin{aligned}\mathcal{G}^{su_1}_{+,x}(s,s_1,s_2) = &\frac{3}{32}\frac{1-3\cos^2\theta}{\lambda}s^2s_1s_2\,[2ss_2\mathcal{L}(s_1;s_2,s)\\ &+s-s_1+s_2]\\ &-\frac{3s}{32}(1+\cos^2\theta)ss_2(s_1+s_2)\mathcal{L}(s_1;s_2,s)\\ &+\frac{ss_2}{64}(1-3\cos^2\theta)(s+s_2-s_1)\\ &+\frac{s}{16}\left[s_1^2-s_2^2-s(s_1+s_2)\right.\\ &\left.-\frac{\lambda\sin^2\theta}{4}\right],\end{aligned} \tag{3.28}$$

$$\begin{aligned}\mathcal{G}^{su_1}_{-,y}(s,s_1,s_2) = &\frac{3}{32}\frac{\cos\theta}{\sqrt{\lambda}}ss_1s_2\left\{2ss_2[2s-(s_1+s_2)]\right.\\ &\times\mathcal{L}(s_1;s_2,s)-2s_2^2+2s_1s_2\\ &\left.+3ss_2-ss_1+s^2\right\},\end{aligned} \tag{3.29}$$

$$\begin{aligned}\mathcal{G}^{su_1}_{+,y}(s,s_1,s_2) = &\frac{ss_1s_2}{64}\left\{6\frac{1-3\cos^2\theta}{\lambda}ss_2\left\{s[s-(s_1+s_2)]\right.\right.\\ &\times\left.\mathcal{L}(s_1;s_2,s)+s+s_1-s_2\right\}\\ &+(1-3\cos^2\theta)[s-2ss_2\mathcal{L}(s_1;s_2,s)]\\ &-16ss_2\mathcal{L}(s_1;s_2,s)\\ &\left.-8(s-s_1+s_2)\right\},\end{aligned} \tag{3.30}$$

$$\begin{aligned}\mathcal{G}^{su_1}_{-,z}(s,s_1,s_2) = &\frac{1}{32}\frac{\cos\theta}{\sqrt{\lambda}}s\left\{6ss_1s_2[2ss_2\mathcal{L}(s_1;s_2,s)\right.\\ &+s-s_1+s_2]\\ &+\lambda\,[6ss_2(s_1+s_2)\mathcal{L}(s_1;s_2,s)\\ &\left.+s(2s_1+3s_2)-s_1s_2-2s_1^2+3s_2^2]\right\},\end{aligned} \tag{3.31}$$

$$\begin{aligned}\mathcal{G}^{su_1}_{+,z}(s,s_1,s_2) = &\frac{3}{64}(1+\cos^2\theta)ss_2\left\{2s[s_1^2\right.\\ &+s_2^2-s(s_1+s_2)]\mathcal{L}(s_1;s_2,s)\\ &\left.+s_2^2-(s+s_1)^2\right\},\end{aligned} \tag{3.32}$$

$$\mathcal{G}^{su_1}_{-,\delta}(s,s_1,s_2) = \mathcal{G}^{su_1}_{-}(s,s_1,s_2), \tag{3.33}$$

$$\mathcal{G}^{su_1}_{+,\delta}(s,s_1,s_2) = \mathcal{G}^{su_1}_{+}(s,s_1,s_2). \tag{3.34}$$

The remaining kinematical functions can be calculated with the equations

$$\begin{aligned}\mathcal{G}^{sd_1}_{\pm,a}(s,s_1,s_2) &= \mathcal{G}^{sd_2}_{\pm,a}(s,s_2,s_1) = \pm\mathcal{G}^{su_2}_{\pm,a}(s,s_2,s_1)\\ &= \pm\mathcal{G}^{su_1}_{\pm,a}(s,s_1,s_2),\end{aligned} \tag{3.35}$$

$$\begin{aligned}\mathcal{G}^{sd_1}_{\pm,z}(s,s_1,s_2) &= \mathcal{G}^{sd_2}_{\pm,z}(s,s_2,s_1) = \mp\mathcal{G}^{su_2}_{\pm,z}(s,s_2,s_1)\\ &= \mp\mathcal{G}^{su_1}_{\pm,z}(s,s_1,s_2),\end{aligned} \tag{3.36}$$

where a stands for x_γ, x_Z, y_γ, y_Z, and δ_Z.

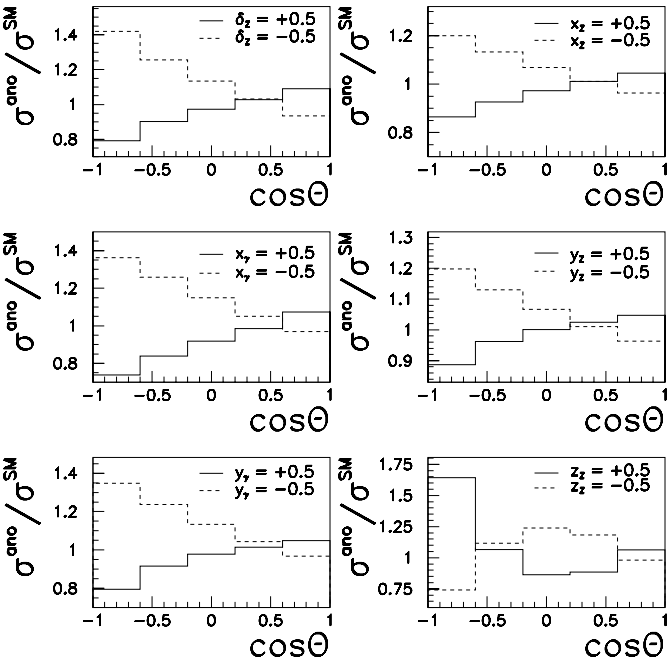

Fig. 5. The ratio of cross-sections with anomalous couplings to standard model cross-sections without background and without ISR corrections at $\sqrt{s} = 190$ GeV. In each figure only one anomalous coupling differs from zero

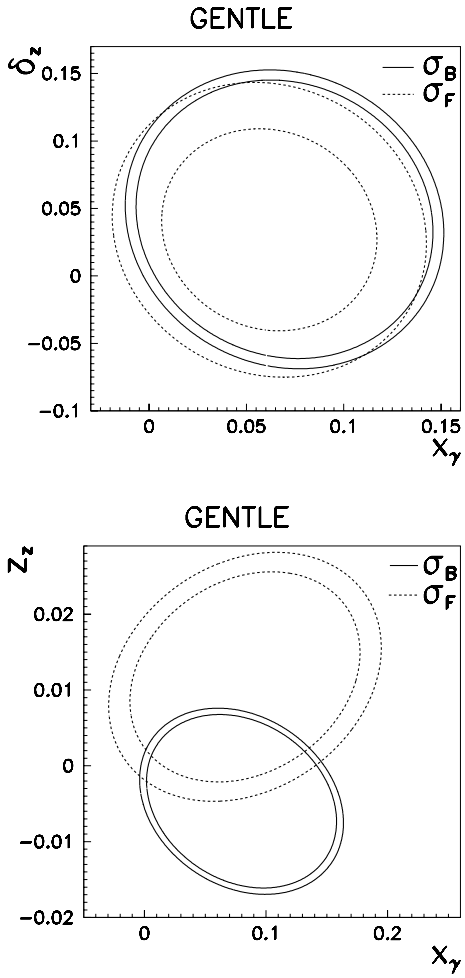

Fig. 6. 1σ-bounds at 500 GeV for $\mathcal{L} = 50$ fb^{-1}

3.3 Numerical results

In Fig. 5 we show the bin-integrated differential cross-section for all the six anomalous couplings at 190 GeV. In each case only one anomalous coupling is allowed to differ from zero. The figure is in excellent agreement with an analogous figure in [43]. Comparisons with the Monte Carlo event generator WOPPER [45,46] show also agreement within the statistical accuracy of the MC program.

As an application, we shortly describe a study on the discriminative power of W pair production with respect to parity conserving and violating anomalous triple boson couplings. At $\sqrt{s} = 500$ GeV with an integrated luminosity $\mathcal{L} = 50$ fb^{-1}, about 80 000 semi-leptonic W pair decays are produced. The anomalous couplings appear in the cross-section at most bilinearly. Allowing e.g. for two anomalous couplings A and B simultaneously, one may use the ansatz:

$$\sigma_{theor} = \sigma^{\rm SM} + A\sigma_1 + A^2\sigma_{11} + B\sigma_2 + B^2\sigma_{22} + AB\sigma_{12}. \quad (3.37)$$

After having calculated $\sigma^{\rm SM}, \sigma_1, \sigma_{11}, \ldots$ with GENTLE (or another program) within a given model and for definite experimental conditions, one may confront experimental data with the predictions. For a study of sensitivities, we use σ_{theor} for the simulation of $\sigma_{meas} \pm \sqrt{\sigma_{meas}/(6\mathcal{L})}$, the assumed measured cross-section with 1σ deviations of the counting rates for the sum of all six semi-leptonic production channels. For definiteness we use for σ_{meas} the standard model prediction $\sigma^{\rm SM}$ and apply no experimental cuts. The solutions of (3.37) for A and B are ellipses in the plane. Allowed pairs of coupling values are located in the area between the two limiting ellipses. For the sample analysis, we use two observables: σ_F and σ_B, the forward and backward cross-sections. The forward (backward) cross-section is defined by the requirement that the angle between the momenta of the e^- and the W^- is less (more) than 90°. We choose these observables since they may be used to form the total cross-section $\sigma_{tot} = \sigma_F + \sigma_B$ (arising from cross-section parts even in the production angle) and the forward backward asymmetry $A_{FB} = (\sigma_F - \sigma_B)/\sigma_{tot}$ (arising from odd cross-section parts). For two different sets of anomalous couplings, the two rings with allowed values derived from σ_F and σ_B overlap almost totally in the case of $\mathcal{P}$ conserving couplings x_γ, δ_Z. When replacing δ_Z by the $\mathcal{P}$ violating coupling z_Z, the allowed ranges overlap much less since the forward-backward asymmetry is more sensitive to this coupling. All this is nicely seen in Fig. 6 (where we also took ISR into account). There, one further may notice that σ_B is more sensitive to anomalous couplings than σ_F although the relative statistical error of the latter is much smaller. This is in accordance with the properties of the angular distributions in Fig. 5 (see also Fig. 2 in [42] for a center-

of-mass energy of 500 GeV). A similar discussion has been performed for other pairs of anomalous couplings in [47].

4 Summary

We determined semi-analytical background and anomalous contributions to the differential cross-section for W pair production in processes of the CC11 class. With the W production angle as an additional parameter, the expressions are not as compact as those for the total cross-section.

By performing numerical calculations with the GENTLE package we illustrated the effects of the background contributions. At energies of about 500 GeV or more, background has sizeable effects especially for backward scattering. At energies of about 190 GeV background is less than 0.3% for all scattering angles. Contributions from anomalous couplings are strongest in the same region. Therefore, they cannot be studied without taking background properly into account.

The present calculation has several limitations, of more importance at higher energies: the virtual corrections are not taken into account; for angular distributions, the QED ISR radiator function used is only an approximation for the real photonic corrections (both with respect to the $O(\alpha)$ part and to higher order corrections); the treatment of finite width effects may be refined. One should estimate the net effect to be of the order of up to few per cent at $\sqrt{s} = 500$ GeV. Thus, GENTLE is certainly an appropriate tool for the study of W pair production at LEP 2 while at higher energy it may serve as a playing ground for sensitivity studies but may not replace a more complete calculation.

Acknowledgement. We would like to thank Th. Ohl for numerous discussions, hints, and numerical comparisons with the Fortran program WOPPER [45,46]. Further, we would like to thank D. Bardin for the continuous fruitful collaboration in the GENTLE project.

A The CC03 process

The coefficient functions used in (2.2) are:

$$\begin{aligned}\mathcal{C}^t = {} & \frac{2}{(6\pi^2)^2}\mathrm{Re}\frac{1}{|D_W(s_1)|^2|D_W(s_2)|^2} \\ & \times L^4(e,W))L^2(F_1,W)L^2(F_2,W) \\ & \times N_c(F_1)N_c(F_2), \end{aligned} \tag{A.1}$$

$$\begin{aligned}\mathcal{C}^{st} = {} & \sum_{k=\gamma,Z}\frac{2}{(6\pi^2)^2}\mathrm{Re}\frac{1}{|D_W(s_1)|^2|D_W(s_2)|^2 D_k(s)} \\ & \times g_k L(e,l)L^2(F_1,W)L^2(F_2,W)L^2(e,W) \\ & \times N_c(F_1)N_c(F_2), \end{aligned} \tag{A.2}$$

$$\begin{aligned}\mathcal{C}^s = {} & \sum_{k,l=\gamma,Z}\frac{2}{(6\pi^2)^2}\mathrm{Re}\frac{1}{|D_W(s_1)|^2|D_W(s_2)|^2 D_k(s)D_l^*(s)} \\ & \times g_k g_l[L(e,k)L(e,l)+R(e,k)R(e,l)] \\ & \times L^2(F_1,W)L^2(F_2,W)N_c(F_1)N_c(F_2). \end{aligned} \tag{A.3}$$

The denominators of the boson propagators are:

$$D_V(s) = s - M_V^2 + iM_V\Gamma_V, \tag{A.4}$$

and the coupling constants in the standard model are:

$$\begin{aligned} & g_\gamma = gs_W = e, \qquad g_Z = gc_W, \\ & L(f,W) = \frac{g}{2\sqrt{2}}, \qquad R(f,W) = 0, \\ & L(f,\gamma) = \frac{eQ_f}{2}, \qquad L(f,Z) = \frac{e}{4s_Wc_W}(2I_3^f - 2Q_f s_W^2), \\ & R(f,\gamma) = \frac{eQ_f}{2}, \qquad R(f,Z) = \frac{e}{4s_Wc_W}(-2Q_f s_W^2). \end{aligned} \tag{A.5}$$

We use $Q_e = -1$ and $I_3^e = -\frac{1}{2}$. The colour factor N_c is 1 for leptons and 3 for quarks.

For the kinematical functions $\mathcal{G}$ we quote the expressions from [36]:

$$\mathcal{G}^t = \frac{1}{8}\left[2s(s_1+s_2) + \frac{\lambda}{4}\sin^2\theta + \frac{\lambda s_1 s_2 \sin^2\theta}{t_\nu^2}\right], \tag{A.6}$$

$$\begin{aligned}\mathcal{G}^{st} = {} & \frac{1}{8}\left[(s-s_1-s_2)\left(2s(s_1+s_2)+\frac{\lambda}{4}\sin^2\theta\right)\right. \\ & \left. -\frac{s_1s_2}{t_\nu}\left(4s(s_1+s_2)-\lambda\sin^2\theta\right)\right], \end{aligned} \tag{A.7}$$

$$\mathcal{G}^s = \frac{1}{32}\lambda\left[2s(s_1+s_2) + \left(3s_1s_2+\frac{\lambda}{4}\right)\sin^2\theta\right], \tag{A.8}$$

with

$$\lambda = s^2 + s_1^2 + s_2^2 - 2ss_1 - 2ss_2 - 2s_1s_2 \tag{A.9}$$

and the denominator of the neutrino propagator t_ν:

$$t_\nu = \frac{1}{2}\left(s - s_1 - s_2 - \sqrt{\lambda}\cos\theta\right). \tag{A.10}$$

B QED corrections

The differential cross-sections are calculated in the rest system Σ' of the W boson pairs (or, equivalently, of the final state fermion pairs). If energetic photons are radiated from the initial state, Σ' differs from the laboratory system Σ where the production angles are determined experimentally. The corresponding Lorentz boost will be described in appendix B.2. An emission of photons from e^- or e^+ leads to different relations between the W production angle in Σ and in Σ'. Thus, we have to use the structure function approach for a description of ISR since here the energy loss of each initial state particle is known.

B.1 Structure function approach

In the structure function approach [48,10], the initial state photonic corrections are taken into account by convoluting the tree-level cross-section twice with the structure function $D(x,s)$ (with the structure functions as described in Sect. 2.3 of [38] and references therein):

$$\frac{\mathrm{d}\sigma_{\mathrm{QED}}(s)}{\mathrm{d}s_1\mathrm{d}s_2\mathrm{d}\cos\theta} = \int_{x_1^{\min}}^{1}\mathrm{d}x_1 \int_{x_2^{\min}}^{1}\mathrm{d}x_2 D(x_1,s)D(x_2,s) \times \sum_{i=1,2}\left|\frac{\mathrm{d}\cos\theta_i'}{\mathrm{d}\cos\theta}\right| \frac{\mathrm{d}\sigma(x_1x_2s,s_1,s_2)}{\mathrm{d}\cos\theta_i'}, \tag{B.1}$$

with $\theta_i' = \theta_i'(s,s_1,s_2,x_1,x_2,\theta)$ and the lower integration boundaries

$$x_1^{\min} \geq \frac{(\sqrt{s_1}+\sqrt{s_2})^2}{s}, \tag{B.2}$$

$$x_2^{\min} \geq \frac{(\sqrt{s_1}+\sqrt{s_2})^2}{x_1 s}. \tag{B.3}$$

The sum in (B.1) indicates that no, one, or two solutions may exist for θ_i' (defined in Σ') at given values of the parameters in Σ. The Jacobean is easily derived from (B.22):

$$\frac{\mathrm{d}\cos\theta_{1,2}'}{\mathrm{d}\cos\theta} = \frac{\beta_{1,2}(1-v^2)}{\left[\beta_{1,2}^2+v^2(1-\beta_{1,2}^2\sin^2\theta)-2v\beta_{1,2}\cos\theta\right]^{3/2}} \times\left[\beta_{1,2}-v\cos\theta\pm v(1-\cos^2\theta)\frac{1-b^2}{b}\frac{v}{1\pm vb\cos\theta}\right]. \tag{B.4}$$

The b is given in (B.21), the velocity v of the W^+W^- system in the laboratory frame Σ in (B.11), and the velocities $\beta_{1,2}$ of the W^- in Σ in (B.16). For doubly resonant diagrams the cross-section has to be multiplied by the Coulomb correction $C(x_1x_2s)$ [49–51]; we follow [50] as described in [36].

For applications and comparisons with Monte Carlo programs [52,53] it might be more convenient to determine not the differential cross-section itself but to perform a bin-wise integration:

$$\sigma = \sum_i \int_{\cos\theta'_{a_i}(\theta_a)}^{\cos\theta'_{b_i}(\theta_b)} \frac{d\sigma}{d\cos\theta'}. \tag{B.5}$$

Such an integration may be trivially performed analytically in Σ' in view of the relatively simple angular dependencies and computer time may be saved. Of course, the boosted integration boundaries have to be determined. For a given angular bin in the laboratory system, there may exist zero, one, or two bins to be integrated over in the boosted frame. More details on this may be found in Sect. 2.4 of [38]. The bin-integrated cross-sections are used in GENTLE for CC03 processes.

Finally, a remark on the use of the structure function $D(x,s)$ might be necessary. This structure function is determined for the total cross-section only. Thus, for the differential cross-section it has to be considered as an approximation.

B.2 Lorentz boost

We will denote 4-momenta in Σ' as p' and in Σ as p. In Σ, the momenta of electron and positron are:

$$p_{e^-} = Ex_1(1,0,0,1), \tag{B.6}$$

$$p_{e^+} = Ex_2(1,0,0,-1). \tag{B.7}$$

$E=\sqrt{s}/2$ denotes the beam energy. In Σ', the sum of the spatial momenta of the two particles vanishes and one gets in this frame:

$$p'_{e^-} = E\sqrt{x_1x_2}(1,0,0,1), \tag{B.8}$$

$$p'_{e^+} = E\sqrt{x_1x_2}(1,0,0,-1). \tag{B.9}$$

Applying the transformation formula

$$p_3' = \frac{p_3 - vp_0}{\sqrt{1-v^2}} \tag{B.10}$$

on one of the beam particles, one may derive the relative velocity of the two Lorentz frames

$$v = \frac{x_1-x_2}{x_1+x_2}. \tag{B.11}$$

In Σ', one may choose the momenta of the W bosons as follows:

$$p'_{W^-} = \left(\sqrt{\frac{\lambda'}{4s'}+s_1},\ \sqrt{\frac{\lambda'}{4s'}}\sin\theta',\ 0,\ \sqrt{\frac{\lambda'}{4s'}}\cos\theta'\right), \tag{B.12}$$

$$p'_{W^+} = \left(\sqrt{\frac{\lambda'}{4s'}+s_2},\ -\sqrt{\frac{\lambda'}{4s'}}\sin\theta',\ 0,\ -\sqrt{\frac{\lambda'}{4s'}}\cos\theta'\right), \tag{B.13}$$

where $s'=4x_1x_2E^2$ is the reduced center-of-mass energy and

$$\lambda' \equiv \lambda(s',s_1,s_2). \tag{B.14}$$

The energy and momenta of the bosons are fixed for given values of s_1 and s_2. The momentum of the W^- boson in Σ can be written as:

$$p_{W^-} = (Q_i, B_i\sin\theta, 0, B_i\cos\theta), \tag{B.15}$$

where Q_i and B_i are real and positive functions of s', s_1, s_2, $\cos\theta$ and v. The velocity of the W^--boson in the laboratory system is then:

$$\beta_i = \frac{B_i}{Q_i}, \qquad i=1,2. \tag{B.16}$$

With

$$p_{e^-} + p_{e^+} = p_{W^-} + p_{W^+} \tag{B.17}$$

and

$$p^2_{W^-} = s_1, \qquad p^2_{W^+} = s_2, \tag{B.18}$$

two sets of solutions may be obtained:

$$B_{1,2} = \frac{(s' - s_2 + s_1)\sqrt{1-v^2}\,(v\cos\theta \pm b)}{2\sqrt{s'}(1 - v^2\cos^2\theta)}, \tag{B.19}$$

$$Q_{1,2} = \frac{(s' - s_2 + s_1)\sqrt{1-v^2}\,(1 \pm bv\cos\theta)}{2\sqrt{s'}(1 - v^2\cos^2\theta)}. \tag{B.20}$$

Here, we used the abbreviation

$$b = \sqrt{1 - \frac{4s_1 s'(1 - v^2\cos^2\theta)}{(s' - s_2 + s_1)^2(1-v^2)}}. \tag{B.21}$$

The number of solutions depends on $\cos\theta$, v and b. By definition, B is real and positive. There is no solution, when $v\cos\theta < -b$, one solution for $|v\cos\theta| < b$, and two solutions exist for $v\cos\theta > b$.

With the given solutions for B and Q and (B.10), the relation between the W production angles in the two Lorentz systems is found:

$$\cos\theta' = \frac{B\cos\theta - vQ}{\sqrt{(1-v^2)B^2\sin^2\theta + (B\cos\theta - vQ)^2}}. \tag{B.22}$$

For the limiting case of on-shell W pair production the transformation (B.22) is in accordance with a similar transformation given in [54].

C Neutral current kinematical functions

In Sect. 2.2.3, we use two kinematical functions known from the the study of neutral current process [55]:

The function $\mathcal{G}^{DD}_{422}$ is:

$$\begin{aligned}\mathcal{G}^{DD}_{422}(\cos\theta; s_1; s_2, s) &= \frac{3}{8}(1+\cos^2\theta)\mathcal{G}_{422}(s_1; s_2, s)\\ &+\frac{1-3\cos^2\theta}{\lambda}s_1(s+s_2)\\ &\times\frac{3}{4}\left(1 - 2\mathcal{L}(s_1; s_2, s)\frac{ss_2}{s_1 - s_2 - s}\right),\end{aligned} \tag{C.1}$$

where $\mathcal{G}_{422}$ is also known from different contexts ([9],[56]-[61]):[1]

$$\mathcal{G}_{422}(s; s_1, s_2) = \frac{s^2 + (s_1+s_2)^2}{s - s_1 - s_2}\mathcal{L}(s; s_1, s_2) - 2. \tag{C.2}$$

The function $\mathcal{G}^{DD}_{233}(\cos\theta, s, s_1, s_2)$ is:

$$\begin{aligned}\mathcal{G}^{DD}_{233}(\cos\theta, s, s_1, s_2) &= \frac{3}{8}(1+\cos^2\theta)\mathcal{G}_{233}(s; s_1, s_2)\\ &-\frac{3}{\lambda^2}\frac{3}{8}(1-3\cos^2\theta)s[\mathcal{L}(s_1; s_2, s)2s_2(s_1 - s_2)\\ &+(s - s_1 - 3s_2)]\\ &\times[\mathcal{L}(s_2; s, s_1)2s_1(s_2 - s_1) + (s - s_2 - 3s_1)],\end{aligned} \tag{C.3}$$

with [37]

$$\begin{aligned}\mathcal{G}_{233}(s; s_1, s_2) &= \frac{3}{\lambda^2}\{\mathcal{L}(s_2; s, s_1)\mathcal{L}(s_1; s_2, s)\\ &\times 4s\left[ss_1(s-s_1)^2 + ss_2(s-s_2)^2 + s_1s_2(s_1-s_2)^2\right]\\ &+(s+s_1+s_2)\left[\mathcal{L}(s_2; s, s_1)2s\right.\\ &\times\left[(s-s_2)^2 + s_1(s+s_2-2s_1)\right]\\ &+\mathcal{L}(s_1; s_2, s)2s\left[(s-s_1)^2 + s_2(s+s_1-2s_2)\right]\\ &\left.+5s^2 - 4s(s_1+s_2) - (s_1-s_2)^2\right]\}.\end{aligned} \tag{C.4}$$

[1] We explicitely agree with [9,56,57]

References

1. S. L. Glashow, Nucl. Phys. **22** (1961) 579
2. S. Weinberg, Phys. Rev. Lett. **19** (1967) 1264
3. A. Salam, *Weak and Electromagnetic Interactions*, in Proc. of the Nobel Symposium, 1968, Lerum, Sweden (N. Svartholm, ed.), pp. 367–377, Almqvist and Wiksell, Stockholm, 1968
4. V. Flambaum, I. Khriplovich, O. Sushkov, Sov. J. Nucl. Phys. **20** (1975) 537–540
5. W. Alles, C. Boyer, A. J. Buras, Nucl. Phys. B **119** (1977) 125
6. Y.-S. Tsai, A. C. Hearn, Phys. Rev. **140** (1965) B721–B729
7. T. Muta, R. Najima, S. Wakaizumi, Mod. Phys. Lett. A **1** (1986) 203
8. F. A. Berends, R. Pittau, R. Kleiss, Nucl. Phys. B **424** (1994) 308–342
9. D. Bardin, M. Bilenky, D. Lehner, A. Olchevski, T. Riemann, Nucl. Phys. (Proc. Suppl.) 37B (1994) 148–157
10. W. Beenakker et al., *WW cross-sections and distributions*, in Physics at LEP2, CERN 96–01 (1996) (G. Altarelli, T. Sjöstrand, F. Zwirner, eds.), pp. 79–139
11. D. Bardin, S. Riemann, T. Riemann, Z. Phys. C **32** (1986) 121
12. F. Jegerlehner, Z. Phys. C **32** (1986) 425; E: ibid., C **38** (1988) 519
13. W. Beenakker, F. Berends, M. Böhm, A. Denner, H. Kuijf, T. Sack, Nucl. Phys. B **304** (1988) 463
14. J. Fleischer, F. Jegerlehner, M. Zralek, Z. Phys. C **42** (1989) 409
15. A. Denner, T. Sack, Z. Phys. C **46** (1990) 653
16. W. Beenakker, K. Kolodziej, T. Sack, Phys. Lett. B **258** (1991) 469–474
17. S. Dittmaier, M. Böhm, A. Denner, Nucl. Phys. B **376** (1992) 29–51
18. J. Fleischer, K. Kolodziej, F. Jegerlehner, Phys. Rev. D **47** (1993) 830–836
19. W. Beenakker, A. P. Chapovsky, F. A. Berends, Phys. Lett. B **411** (1997) 203
20. W. Beenakker, A. P. Chapovsky, F. A. Berends, Nucl. Phys. B **508** (1997) 17
21. A. Denner, S. Dittmaier, M. Roth, Nucl. Phys. B **519** (1998) 39
22. K. J. F. Gaemers, G. J. Gounaris, Z. Phys. C **1** (1979) 259
23. K. Hagiwara, R. D. Peccei, D. Zeppenfeld, K. Hikasa, Nucl. Phys. B **282** (1987) 253
24. K. Hagiwara, S. Ishihara, R. Szalapski, D. Zeppenfeld, Phys. Rev. D **48** (1993) 2182–2203

25. C. L. Bilchak, J. D. Stroughair, Phys. Rev. D **30** (1984) 1881
26. F. Jegerlehner, Nucl. Phys. (Proc. Suppl.) 37B (1994) 129–140
27. A. M. H. ar Rashid, K. S. Islam, Int. J. Mod. Phys. A **9** (1994) 2783–2804
28. G. Gounaris et al., *Triple gauge boson couplings*, in Physics at LEP2, CERN 96–01 (1996) (G. Altarelli, T. Sjöstrand, F. Zwirner, eds.), pp. 525–576
29. ECFA/DESY LC Physics Working Group Collaboration, E. Accomando et al., Phys. Rept. **299** (1998) 1
30. R. Clare, Acta Phys. Polon. B **29** (1998) 2667
31. J. Ellison, J. Wudka, *Study of trilinear gauge boson couplings at the Tevatron collider*, UC Riverside preprint UCR-D0-98-01 (1998), subm. to Ann. Rev. Nucl. Part. Sci. `e-print hep-ph/9804322`
32. CDF and D0 Collaborations, J. Ellison, *Measurements of the W boson mass and trilinear gauge boson couplings at the Tevatron*, UC Riverside preprint UCR-D0-98-21, June 1998, to be published in Proc. XXXIII^d Rencontres de Moriond, Electroweak Interactions and Unified Theories, Les Arcs, Savoie, France, March 14-21 1998 `e-print hep-ex/9806004`
33. G. Gounaris, C. Papadopoulos, *Studying Trilinear Gauge Couplings in $e^+e^- \to l^-\bar{\nu}_l q\bar{q}'$ at Linear Collider Energies*, in *e^+e^- Linear Colliders: Physics and Detector Studies - Part E,* DESY 97-123E (1997) (R. Settles, ed.), p. 143
34. D. Bardin, A. Olshevsky, M. Bilenky, T. Riemann, Phys. Lett. B **308** (1993) 403–410; E: ibid., B **357** (1995) 725
35. D. Bardin, D. Lehner, T. Riemann, Nucl. Phys. B **477** (1996) 27–58
36. D. Bardin, T. Riemann, Nucl. Phys. B **462** (1996) 3–28
37. D. Bardin, A. Leike, T. Riemann, Phys. Lett. B **344** (1995) 383–390
38. D. Bardin, J. Biebel, D. Lehner, A. Leike, A. Olchevski, T. Riemann, Comput. Phys. Commun. **104** (1997) 161. `GENTLE` is available at `http://www.ifh.de/theory/publist.html`
39. J. A. M. Vermaseren, *Symbolic Manipulation with* `FORM` (Computer Algebra Nederland, Amsterdam, 1991)
40. E. N. Argyres et al., Phys. Lett. B **358** (1995) 339–346
41. W. Beenakker et al., Nucl. Phys. B **500** (1997) 255
42. J. Biebel, *Four fermion production with anomalous couplings at LEP 2 and NLC*, in *Proc. of XIIth International Workshop on High Energy Physics and Quantum Field Theory, 4–10 Sep 1997, Samara, Russia* (B. Levtchenko, ed.), 1998, to appear; **e-print hep-ph/9711439**
43. F. A. Berends, A. I. van Sighem, Nucl. Phys. B **454** (1995) 467–484
44. H. Aronson, Phys. Rev. **186** (1969) 1434–1441
45. H. Anlauf, J. Biebel, H. Dahmen, A. Himmler, P. Manakos, T. Mannel, W. Schönau, Comput. Phys. Commun. **79** (1994) 487–502
46. H. Anlauf, P. Manakos, T. Ohl, H. Dahmen, `WOPPER`, *version 1.5: A Monte Carlo event generator for $e^+e^- \to (W^+W^-) \to 4f + n\gamma$ at LEP-2 and beyond*, Darmstadt preprint IKDA 96–15 (1996), `e-print hep-ph/9605457`
47. J. Biebel, T. Riemann, *Semianalytic predictions for W pair production at 500 GeV*, in *e^+e^- Linear Colliders: Physics and Detector Studies - Part E,* DESY 97-123E (1997) (R. Settles, ed.), p. 139
48. E. A. Kuraev, V. S. Fadin, Sov. J. Nucl. Phys. **41** (1985) 466–472
49. V. S. Fadin, V. A. Khoze, A. D. Martin, Phys. Lett. B **311** (1993) 311–316
50. D. Bardin, W. Beenakker, A. Denner, Phys. Lett. B **317** (1993) 213–217
51. V. S. Fadin, V. A. Khoze, A. D. Martin, A. Chapovsky, Phys. Rev. D **52** (1995) 1377–1385
52. D. Bardin et al., *Event generators for WW physics*, in *Physics at LEP2,* CERN 96–01 (1996) (G. Altarelli, T. Sjöstrand, F. Zwirner, eds.), vol. 2, pp. 3–353
53. T. Ohl, Acta Phys. Polon. B **28** (1997) 847
54. W. Beenakker, F. A. Berends, W. L. van Neerven, *Applications of renormalization group methods to radiative corrections*, in *Proc. of Workshop on Electroweak Radiative Corrections for e+ e- Collisions, 3–7 April 1989, Tegernsee, Germany* (J. H. Kühn, ed.), pp. 3–24, Springer-Verlag, Berlin, 1989
55. A. Leike, *Semianalytic distributions in four fermion neutral current processes*, in *Proc. of Int. Workshop on Perspectives for Electroweak Interactions in e^+e^- Collisions, 5–8 Feb. 1995, Tegernsee, Germany* (B. Kniehl, ed.), pp. 121–130, World Scientific, Singapore, 1995
56. V. Baĭer, V. Fadin, V. Khoze, Sov. J. Nucl. Phys. **23** (1966) 104–111
57. M. Cvetič, P. Langacker, Phys. Rev. D **46** (1992) 4943–4954
58. R. Stuart, *Gauge invariance in boson production*, in Proc. of Int. Workshop on the Higgs Puzzle, 8–13 Dec. 1996, Tegernsee, Germany (B. Kniehl, ed.), pp. 47–54, World Scientific, Singapore, 1996
59. R. Stuart, *Unstable particles*, in Proc. of Int. Workshop on Perspectives for Electroweak Interactions in e^+e^- Collisions, 5–8 Feb. 1995, Tegernsee, Germany (B. Kniehl, ed.), pp. 235–246, World Scientific, Singapore, 1995
60. R. Stuart, *Gauge invariance and the unstable particle*, talks at *Workshop on Hadron Production Cross-Sections at DAPHNE meeting, 1–2 Nov 1996, Karlsruhe, Germany*, and at *1st Latin American Symposium on High-energy Physics,* SILAFAE-I*, 1–5 Nov 1996, Merida, Mexico*, unpublished, e-print `hep-ph/9706550`
61. R. Stuart, Nucl. Phys. B **498** (1997) 28